CHALMERS
UNIVERSITY OF TECHNOLOGY

Reduction of surface oxide layers on water-atomized iron and steel powder in hydrogen: Effect of alloying elements and initial powder state

Thermochimica Acta 692 (2020) 178731

Contents lists available at ScienceDirect

Thermochimica Acta

journal homepage: www.elsevier.com/locate/tca

Reduction of surface oxide layers on water-atomized iron and steel powder in hydrogen: Effect of alloying elements and initial powder state

Johan Wendel*, Swathi K. Manchili, Eduard Hryha, Lars Nyborg

Department of Industrial and Materials Science, Chalmers University of Technology, Rännvägen, 2A, 412 96, Gothenburg, Sweden

ARTICLE INFO

Keywords:
Water-atomized iron powder
Water-atomized steel powder
Thermogravimetric analysis
Oxide reduction
Reduction kinetics

ABSTRACT

The reduction of surface oxide layers covering commercial water-atomized iron and steel powder grades have been investigated using model thermogravimetric reduction cycles in hydrogen. The influences of powder composition and initial condition on the oxide reduction were studied for three powder grades and compared to Fe_2O_3. Isothermal and dynamic measurements were conducted to assess the reduction progress and kinetic analyses were then used to calculate the apparent activation energies of reduction. Chromium-alloyed powder showed significantly lower activation energies compared to iron powder and Fe_2O_3, likely originating from the presence of Cr oxide in the oxide layer. The reduction was also found to be strongly affected by the initial state of the oxide layer which reflects the powder production. Surface analysis by X-ray photoelectron spectroscopy (XPS) showed a progressive increase in Cr with gradual reduction of the oxide layer, indicating its presence and possible involvement in the oxide reduction.

1. Introduction

Metal powder particles are covered by thin oxide layers as a result of their exposure to air or oxygen-containing atmospheres. These surface layers account for up to 30–50 % of the total oxygen in typical commercial water-atomized ferrous powder grades used in the powder metallurgy (PM) industry [1], with layer thicknesses commonly reported to be in the range of 5 − 7 nm for plain iron and chromium pre-alloyed grades [1–3]. In addition to the oxide layer, which covers 90–95 % of the powder surface, small oxide particulates enriched in elements like Cr and Mn are distributed on the surfaces of the powder particles. Because the amount of oxygen in the powder translates to unwanted oxide inclusions in the final sintered component, the reduction of oxides, and the subsequent removal of oxygen-containing reaction products, is seen as a major goal in sintering. Failure to remove oxides can have detrimental effects on mechanical properties, such as impact strength and fatigue life [4]. Previous studies of metal oxides in PM material systems have mostly been concerned with the small oxide particulates; see for example [1] regarding the thermodynamic stability and formation of spinel-type oxides containing Cr and Mn oxides or [3–5] for some characteristics regarding the size, composition, distribution and effect on mechanical properties of particulate oxides on chromium-alloyed steels. However, the initial reduction of the iron-rich surface oxide layer has received less attention, the reason being the low thermodynamic stability of the iron oxides relative to that of oxides based on Cr or Mn [1]. Since industrial sintering practise for chromium-alloyed steel uses hydrogen as one component of the processing gas, the iron oxides comprising the major part of the surface oxide layer can be effectively reduced at low temperatures of about 400 °C [1,2], and have not been seen as a major problem. However, it is known that oxides become enclosed by particles when the powder is compacted, and that transfer of oxygen from low-stability oxides to more stable ones makes their removal more difficult during sintering [1,4,6].

The purpose of this study is to investigate the reduction of the surface oxide layers on water-atomized iron and chromium-alloyed steel powder grades. The influence of powder chemistry and the effect of the initial, as-received conditions after powder production are evaluated for commercial powder grades. Oxide layers formed on Fe-Cr alloys at room temperature should reflect the nominal composition [7] which means a difference in oxide composition between the iron and steel powder can be expected. Regarding the initial state, the powder in the as-received condition reflects the production and subsequent handling of the powder which leads to an oxide layer that is different from the native oxide formed on pure Fe which will likely affect the reduction properties. A thermogravimetric analysis (TGA) setup with well-controlled temperature and atmosphere conditions was used for the experiments, something that has proven to be highly successful in studying reduction events during sintering of PM steels, see for example

* Corresponding author.
E-mail address: johan.wendel@chalmers.se (J. Wendel).

https://doi.org/10.1016/j.tca.2020.178731
Received 4 June 2020; Received in revised form 27 July 2020; Accepted 28 July 2020
Available online 02 August 2020

Table 1
Nominal composition of the supplied powder grades.

Powder	Fe	Cr	Mo	O (max)
ASC100.29	Bal.	–	–	0.11
Astaloy CrA	Bal.	1.8	–	0.15
Astaloy CrM	Bal.	3.0	0.5	0.15

[8–11]. Subsequent kinetic analyses based on the Kissinger [12] and an isoconversional method [13] were then applied to study the kinetics of oxide reduction, shown to be applicable for silver oxide [14], nickel oxide [15], iron ores and pure iron oxides [16,17] as well as for water-atomized iron powder [18]. In this way, the effects of powder chemistry and initial surface oxide condition on the reduction kinetics could be revealed. With this information, new insights are provided to the oxide transformation models currently used to describe the heating stage of sintering. As a complement to the thermal analysis, surface analysis by X-ray photoelectron spectroscopy (XPS) was used for analysing the surface chemical state of the chromium-alloyed powder in order to expose any differences in oxide layer composition relative to that of the oxide layer on iron powder.

2. Materials and experimental procedure

Water-atomized iron and steel powder grades were provided by Höganäs AB, Sweden. The tradenames and nominal composition of the grades can be seen in Table 1. The particle sizes are typically in the range 20 − 180 μm. In the following, the acronyms ASC, CrA and CrM will be used.

Apart from the alloying elements, oxygen levels of 0.1 − 0.15 wt. % are typically found. The CrA and CrM powder grades are pre-alloyed with chromium for hardenability. While chromium is considered sensitive to oxygen, its activity is reduced through the pre-alloying to prevent excessive oxidation [19]. In addition to these elements, it should be noted that trace elements such as Mn and Si are present to a lesser degree. As a reference for iron oxide reduction, a pure Fe_2O_3 oxide (hematite powder of 99 % purity with particle size < 5 μm, acquired from Sigma Aldrich) was also used.

An overview of the powder particle size and morphology was acquired using a PHI 700 AES instrument at 10 kV accelerating voltage.

2.1. Thermogravimetric setup

A Netzsch STA 449 *F1 Jupiter®* thermogravimetric analyser with an Al_2O_3 furnace tube and a W-Re thermocouple was used as the sintering furnace for the experiments. High purity (99.9999 %) hydrogen was used as the processing atmosphere to ensure that complete reduction could be achieved without thermodynamic limitations. Approximately 2 g of iron/steel powder or 1 g of oxide powder were put in an Al_2O_3 crucible and loaded into the instrument which was then evacuated and flushed with argon (99.9999 %) to assure the purity of the sintering atmosphere during the experiments. The instrument was then set to an initial standby state for 30 min for balance stabilization during which the hydrogen processing gas becomes active for the remainder of the experimental program. For isothermal measurements, the samples were heated at 10 °C/min to temperatures in the range 250 − 350 °C which is below the expected reduction temperatures. The samples were then held for 30 − 120 min at the designated temperature with longer holding times for isothermal measurements conducted at lower temperatures in order to account for the longer reaction times. For dynamic measurements, the samples were heated to temperatures in the range 500 − 700 °C and immediately cooled down to room temperature without hold. The heating rates (HR) were varied in the range 10 − 50 °C/min to provide the basis for the subsequent kinetic analysis. The cooling rate was kept constant at 30 °C/min down to room temperature for all measurements. Reduction studies of newly formed oxide layer on the powder surfaces at ambient conditions were conducted to investigate the effect of the initial, as-received state of the powder. To do so, repeated dynamic measurements were made where the furnace chamber was opened for about 1 min after the initial reduction trial followed by a subsequent measurement of the reduction of the newly formed surface oxide.

It is acknowledged that several factors linked to the thermogravimetric setup will likely influence the results; (i) some degree of thermal inertia [20] is present although the heat transfer between hydrogen and metal powder is expected to be good, and (ii) hydrogen penetration and water vapor removal will affect the local microclimate in the powder bed. However, since the sample mass is kept at 2 g for all metal powder measurements, any limitations in the setup regarding thermal inertia, hydrogen penetration and microclimate renewal are assumed to be constant which means that any observed differences in the measurements are characteristic of the analysed powder samples.

2.2. Kinetic analyses

The kinetic analyses were done based on the Kissinger and isoconversional methods [12,13] which have previously been successfully applied to investigate reduction of iron oxides in hydrogen [16,17]. Here the methodology is further developed for studying reduction of oxides in an applied setting where they exist as a thin layer covering metal powder particles [18]. The Kissinger approach features a single activation energy, E, based on the temperature positions of the peak rate of mass loss in the first derivative of the thermogravimetric curve according to Eq. 1:

$$\ln\left(\frac{\Phi}{T_m^2}\right) = \text{constant} - \frac{E}{RT_m} \quad (1)$$

where Φ is the heating rate, T_m is the temperature at the peak rate of mass loss and R is the universal gas constant. A plot of $\ln \Phi/T_m^2$ vs. $-E/RT_m$ then gives the activation energy as the slope of the curve. The isoconversional method requires a description of the extent of conversion of each reaction following the formula:

$$\alpha = \frac{m_i - m}{m_i - m_f} \quad (2)$$

where α is the conversion and m_i, m_f and m are the initial, final and instantaneous masses of the samples, respectively. Dynamic measurements with varying heating rates of 10 − 50 °C/min were analysed based on the conversion and then plotted versus the temperature at each conversion step, T_α. The activation energies, E_α, at conversion steps of 0.05 in the range $0.1 \leq \alpha \leq 0.9$ were then extracted from the slopes of the linear regression curves according to the expression:

$$\ln\left(\frac{\Phi}{T_\alpha^2}\right) = \text{constant} - \frac{E_\alpha}{RT_\alpha} \quad (3)$$

2.3. X-ray photoelectron spectroscopy

Surface analysis using X-ray photoelectron spectroscopy (XPS) was done to track the chemical changes that occur during the reduction of the oxide layers on chromium-alloyed powder. This was done by measuring powder heated to intermediate temperatures of the reduction process in the range 250 − 400 °C for CrA, before being immediately cooled down to room temperature. The heating was done using the thermogravimetric setup explained previously. The powder samples were then pressed onto Al-plates prior to XPS measurements which were conducted using a PHI VersaProbe III instrument operated at 50 W. The subsequent analysis was done using the PHI MultiPak software (version 9.7.0.1).

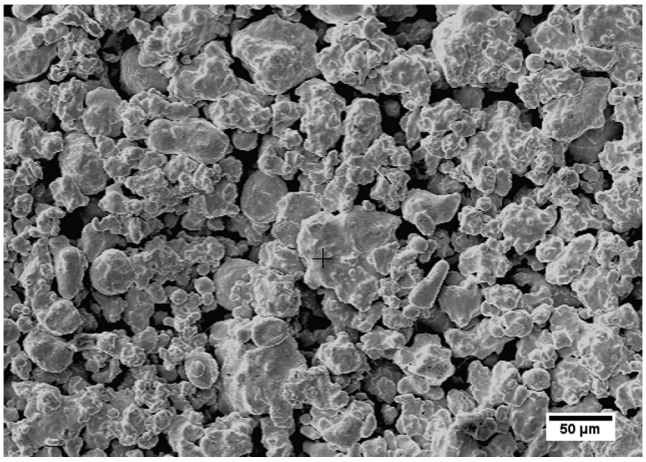

Fig. 1. Overview of as-received water-atomized iron powder.

3. Results and discussion

An overview of the water-atomized iron powder can be seen in Fig. 1, illustrating the typical irregular particle morphology of water-atomized ferrous powder which contributes to its large surface area and reactivity.

3.1. Thermogravimetric analysis

Thermogravimetric curves at a heating rate of 10 °C/min for the three powder grades can be seen in Fig. 2a-b. The mass loss (TG) curves in Fig. 2a show a drop in the range 320 − 400 °C, characteristic for the reduction of the surface oxide layer. This is a commonly observed feature of water-atomized powder heated in hydrogen-containing atmospheres [1,2,21], and is beneficial since the oxide typically contains a large fraction of the total oxygen in the powder [1,2]. The first derivative (differential TG, DTG) curves in Fig. 2b show the rate of mass losses versus temperature. Here it is clearly shown that the overall reduction behaviour changes with powder grade. The peak position of the surface oxide layer reduction occurs at just below 400 °C for plain iron powder, whereas the oxide layers in the case of the chromium-alloyed grades are reduced at significantly lower temperatures of 317 and 335 °C, respectively. The observed differences between the powder grades indicate an influence of the their composition, even though the surface oxide layer on these powder grades are commonly reported to be composed mainly by Fe_2O_3 [1–3]. However, it should be noted that the reported absence of chromium within the surface oxide layer [3] may have been caused by limitations with detecting chromium in low concentrations in nano-sized oxide layers [22].

The Fe_2O_3 and Cr_2O_3 oxides are miscible and may form solid solutions [22], and the oxide formed at room temperature on simple binary Fe-Cr alloys should reflect the alloy composition if the atomic mobility is low [7]. Therefore, it is expected that the surface oxide layers on water-atomized iron and steel powder grades are chemically different. It is then likely that their reduction properties are also different. The thermodynamic requirements for reducing iron oxides (FeO, Fe_3O_4 or Fe_2O_3) are relatively low compared to other oxides commonly encountered in modern PM steelmaking, such as those based on chromium or manganese [1,23]. While the reduction of iron oxides is easily achievable in hydrogen-based atmospheres at low temperatures, additional reducing agents are typically required to reduce oxides based on Cr and Mn, including the mixed Fe, Cr and Mn spinel type oxides that are also present in these material systems and possess intermediary thermodynamic stability [1]. Based on this it could be expected that the reduction would take place at higher temperatures for chromium-alloyed powder while this is clearly not the case, as observed in Fig. 2. Consequently, the change in reduction between the powder grades must be influenced by some other mechanism. One study showed an influence on the reduction properties of chromium-doped iron oxides where the reduction temperature was lowered [24], whereas other studies indicate that reduction is altered in the presence of foreign metal oxides [25–27], with structural factors and metal additives likely playing a role as catalysts for the reduction [28,29]. While the composition of the oxide layer should reflect the composition of the alloy as indicated above, the iron oxide component of the oxide layer is expected to be selectively reduced, thus leaving the more stable chromium oxide remaining as residue on the surface. It is also conceivable that oxygen transfer from iron oxide to chromium at the metal/oxide interface through a metallothermic reduction mechanism can aid in the reduction process, but the magnitude of its contribution to the overall reduction behaviour is difficult to assess. Here it is believed that several factors linked to powder and oxide composition as well as oxide structure could influence the reduction. To further analyse the effect of composition on the reduction of the surface oxide layer, a series of thermogravimetric experiments were conducted under both isothermal and dynamic conditions.

3.1.1. Isothermal reduction

The results from the isothermal experiments can be seen in Fig. 3a-d where the mass losses (3a) and conversions (3b-d) of the oxide layers are plotted versus time at different holding temperatures for all three powder grades. The selection of isothermal temperatures was based on the dynamic reduction peaks in Fig. 2 and is chosen to be − 50 − 100 °C lower, starting from the onset of reduction. In Fig. 3a it can be seen that the mass losses at 300 °C correlate well with the dynamic measurements in Fig. 2 and that about 0.03 % of the mass is lost due to the reduction of the oxide layer. The mass losses are then converted to the extent of conversion according to Eq. 2 and then shown in Fig. 3b as a comparison of the conversion versus time for the grades at 300 °C. Here the time required for complete reduction becomes apparent with CrA reaching full conversion in 15 min, CrM in 25 min and ASC100.29 in 90 min. The chromium-alloyed grades show decelerating reduction curves with a large and rapid initial reduction followed by a diminishing rate of mass loss. The plain iron grade instead shows a constant rate of conversion up to $\alpha = 0.4$ followed by a slight acceleration at $\alpha = 0.4 - 0.6$ before decelerating at $\alpha = 0.8$ for an overall more sigmoidal shape. Fig. 3c-d show how the time for complete conversion changes when the temperature is increased or decreased for ASC100.29 and CrA, respectively. The iron powder shows a decelerating behaviour at high isothermal temperatures but transitions to a more sigmoidal reduction behaviour when the temperature is lowered (3c). In contrast, CrA shows a decelerating trend even at relatively low temperatures (3d) suggesting that the oxide reduction on iron and steel powder follow distinctly different paths under these conditions [13]. The results again indicate that the observed differences between the powder grades reflect the differences in the chemical composition, as detailed in Table 1, although there seems to be no difference between chromium contents of 1.8 or 3 wt. %. Since the oxide layers can be reduced at low temperatures, even down to 250 °C in the case of CrA, this points towards that the reduction processes are mainly governed by kinetic limitations of the reaction itself but also heat transfer and removal of reaction products. Thermodynamic limitations like the temperature and purity of the processing gas appears to be less important in the current thermogravimetric setup, thereby enabling the study of the kinetic parameters.

3.1.2. Dynamic reduction

Results from dynamic measurements, where $dT/dt \neq 0$, can be seen in Fig. 4a-d for the iron powder and Fe_2O_3 at heating rates 10 − 50 °C/min. The iron powder curves all have the same sigmoidal shape of reduction which is then shifted to higher temperatures with increasing heating rates (4a). For the Fe_2O_3 reference, the first reduction step corresponding to the reaction $Fe_2O_3 \rightarrow Fe_3O_4$ is analysed (4c). This step

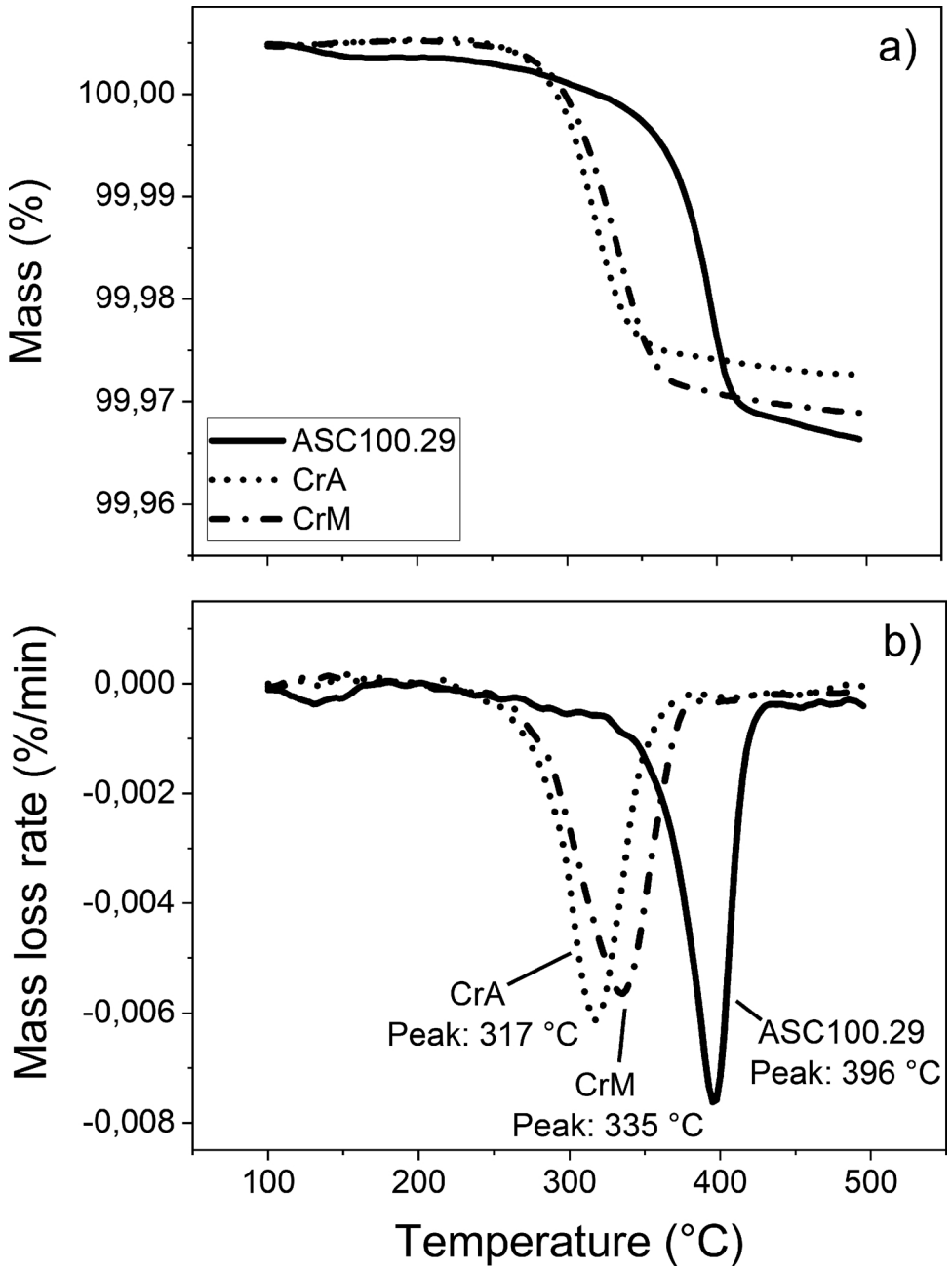

Fig. 2. Thermogravimetric curves of ASC100.29, CrA and CrM up to 500 ˚C.

also follows a sigmoidal curve shape, but with much larger mass losses due to its pure oxide nature. The remaining reduction to metallic iron in Fig. 4c-d is omitted since it takes place at higher temperatures for this reference powder. It should be noted that the differences in mass values in Fig. 4a and d come from the difference in experiment buoyancy when using varying heating rates, but the total mass losses for the respective reduction reactions are still the same.

In Fig. 5, the dynamic measurements for the iron and two chromium-alloyed powder grades are recalculated to the extent of conversion according to Eq. 2. The curves in Fig. 5a-b for ASC100.29 and CrA show the same general behaviour with a clear shift in conversion to higher temperatures at higher heating rates, which forms the basis of the kinetic analyses. Like Figs. 2–3, it is again clear that the reduction temperature is strongly affected by the composition of the powder. Fig. 5c shows a comparison between the powder grades at heating rates of 10 and 50 ˚C/min; at $\alpha = 0.5$ and a heating rate of 10 ˚C/min, the temperature is around 392 ˚C for ASC100.29, 315 ˚C for CrA and 335 ˚C for CrM, respectively. The temperature shifts for reduction are thus in the order of 60 − 80 ˚C between ASC100.29 and the two chromium-alloyed grades. However, even though the temperature shift is large, the sigmoidal appearance of the conversion curves indicate that the reduction mechanisms are similar for all powder grades under the current dynamic reduction conditions.

The results from the dynamic measurements of all samples are used as input for the kinetic analyses as described in the experimental method section. For conversions in the range $\alpha = 0.1 - 0.9$ in steps of 0.05, the temperature at each step is extracted and plotted according to Eq. 3.

3.2. Native oxide

The chosen powder grades are in their commercial, as-received

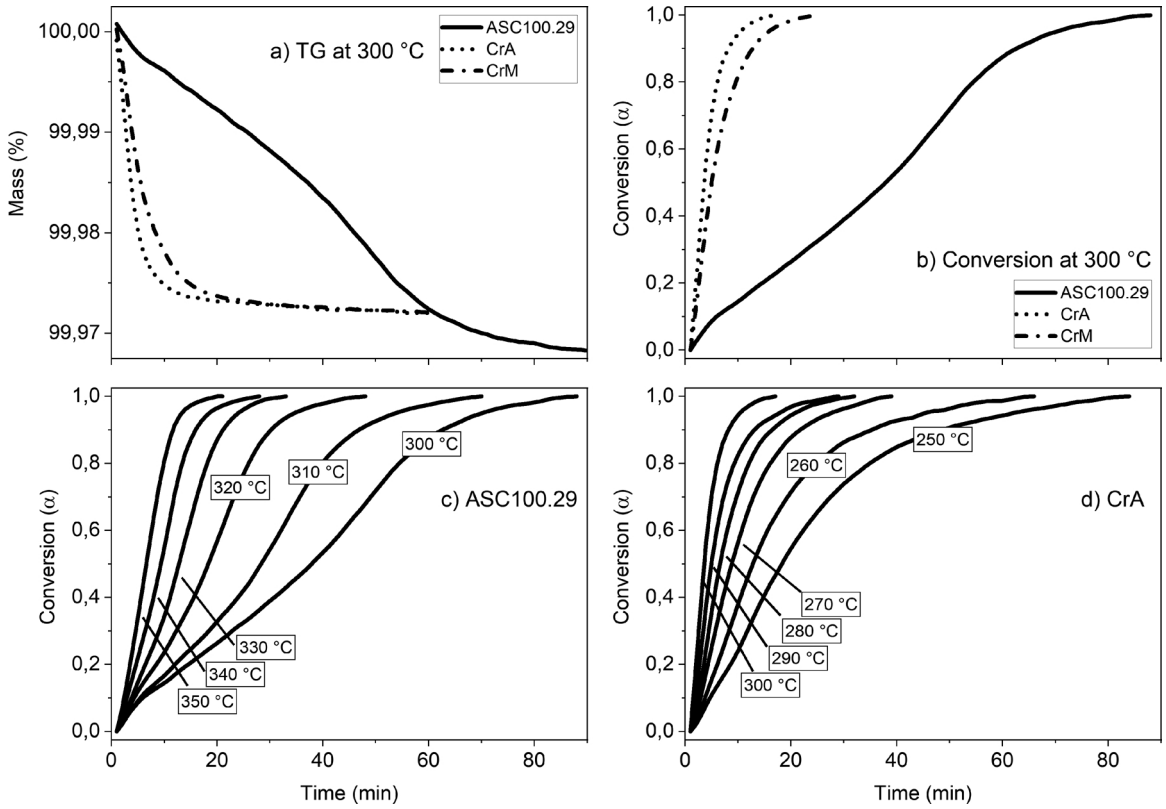

Fig. 3. Isothermal reduction curves showing conversion of ASC100.29, CrA and CrM at different temperatures.

conditions prior to the thermogravimetric measurements. Consequently, the surface oxide layers covering the metal powder particles at this point are typically not identical to the oxides that would otherwise be expected to form on a fresh metal surface when exposed to ambient conditions. The reason for this being the differences in powder production, processing and handling, such as when the metal powder is

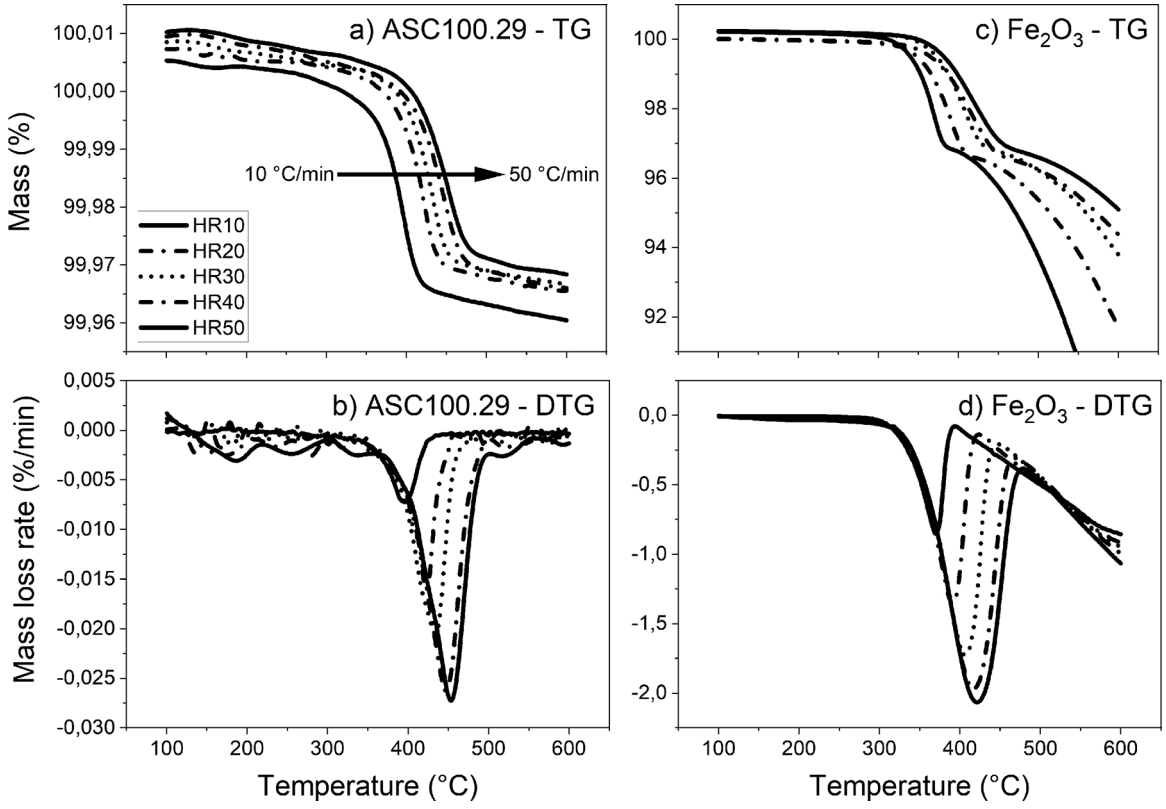

Fig. 4. Dynamic measurements of ASC100.29 and a Fe_2O_3 reference powder.

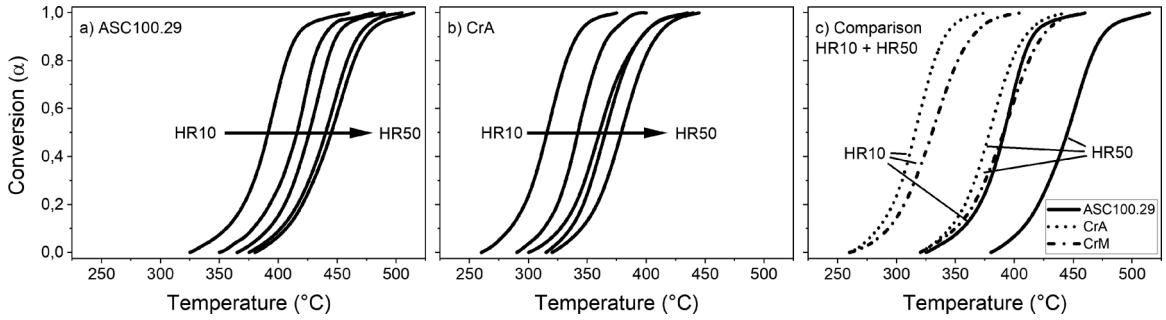

Fig. 5. Conversion versus temperature for ASC100.29, CrA and CrM at different heating rates.

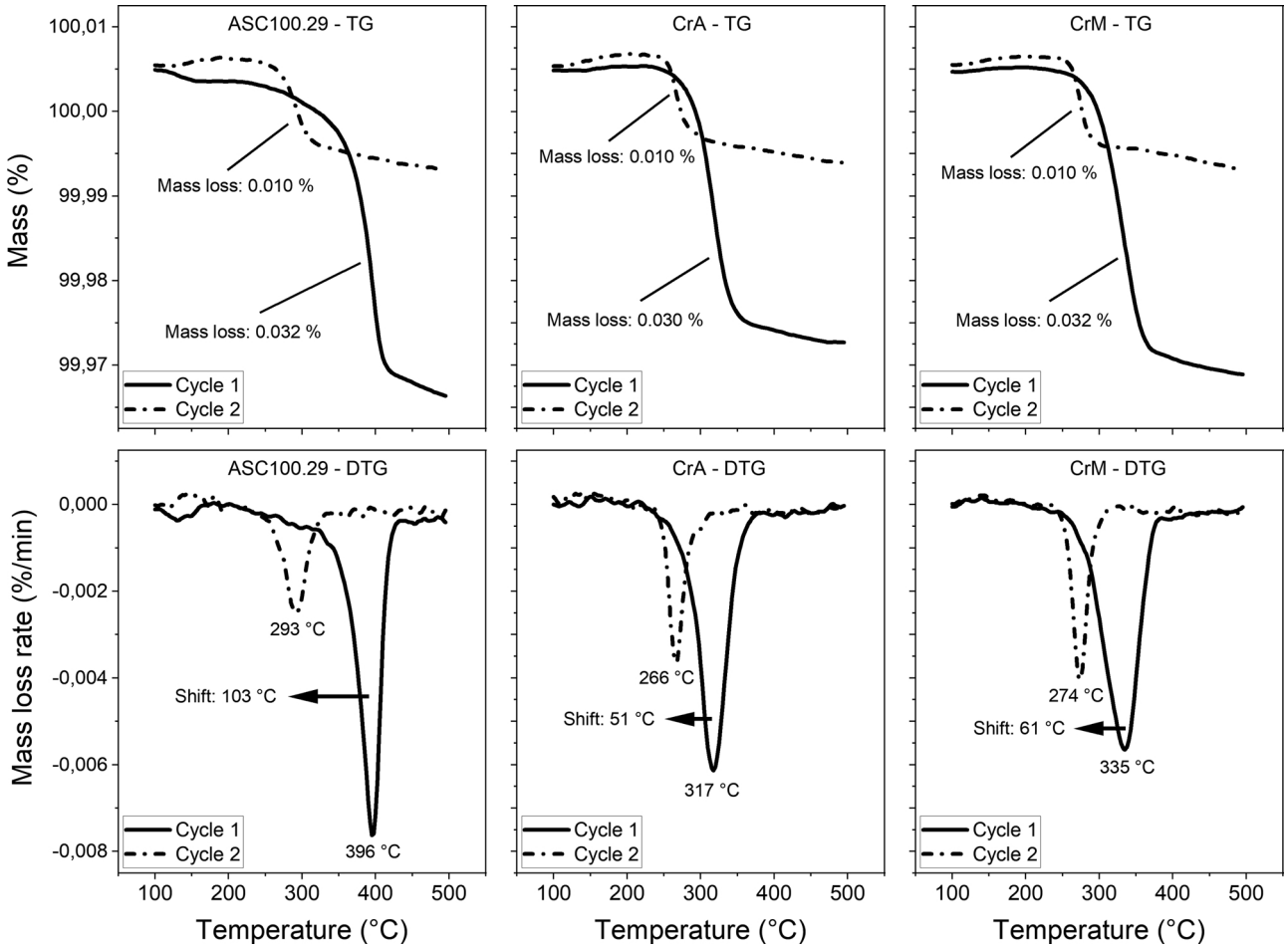

Fig. 6. Reduction of as-received and native oxides formed on powder grades. The reduction peaks are smaller and are shifted to lower temperatures after re-oxidation.

annealed under reducing conditions and subsequently cooled down [1,3]. To investigate the differences between the initial as-received powder and reduced powder, thermogravimetric analyses up to 500 °C were conducted twice for each powder. First a cycle to completely reduce the initial oxide layers and a second cycle to reduce the powder re-oxidized at ambient conditions to analyse the changes in magnitude and temperature position of the reduction peaks. Between each measurement, the furnace chamber was opened after cooling to a temperature of around 30 °C to initiate a re-oxidation of the powder surfaces by air, and then closed after 1 min. The procedure effectively normalizes the powder so that any differences between the powder grades originating from powder production, annealing and handling are removed. The results are shown in Fig. 6 where it can be seen that the magnitude of mass loss is about 3 times smaller for the second cycle for all powder grades. This means that the thickness of the re-oxidized oxide layer can be expected to be significantly smaller than that of the layer on as-received powder, assuming that negligible amounts of surface area reduction due to diffusion has occurred while heating to 500 °C. The native oxide forming on pure iron surfaces at room temperature is typically around 3 nm [30], which would then correspond to the lower limit of the observed thermogravimetric response in Fig. 6, although limitations in air penetration into the powder bed may prevent extensive re-oxidation when the furnace is opened. Meanwhile, the oxide layer thickness for both plain iron and chromium-alloyed powder grades is typically reported to be 6 – 7 nm [2,3], and the results in Fig. 6 further suggest a significant difference in oxide layer thickness after re-oxidation.

Another feature observed in Fig. 6 is that the oxide layer is removed

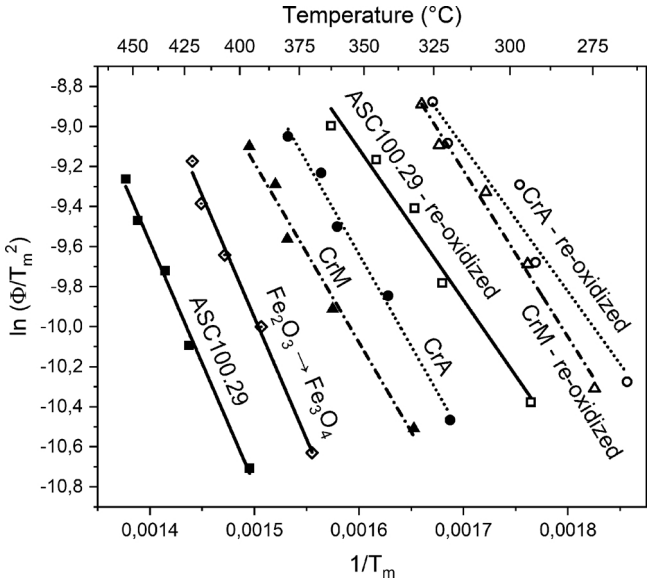

Fig. 7. Kissinger plots for $Fe_2O_3 \rightarrow Fe_3O_4$ and as-received and re-oxidized powder grades.

at significantly lower temperatures for the re-oxidized powder grades; a decrease of more than 100 °C is recorded for the ASC100.29 powder while the CrA and CrM curves are shifted to lower temperatures by about 50 and 60 °C, respectively. The large shifts indicate that the nature of the oxide layers on the as-received powder is significantly different compared to the native oxide layers formed after re-oxidation. As mentioned previously, these differences are likely a consequence of the powder production, processing, and handling. However, the oxide layers show that a difference in reduction temperature remains even after the powder grades are normalized by reduction and re-oxidation, something which indicates the influence of powder composition. Dynamic experiments of the re-oxidised oxide layers with multiple heating rates were conducted for comparison with the as-received powder grades and used in the subsequent kinetic analyses.

3.3. Kinetic analyses of surface oxide layer reduction

The kinetic analyses were done according to the methodology described in the experimental section. The results from the Kissinger analysis are presented in Fig. 7 for all three powder grades in their as-received states as well as for the $Fe_2O_3 \rightarrow Fe_3O_4$ reduction step of the reference oxide powder. Results from re-oxidized powder showing reduction of the native oxides are also included. Fig. 7 essentially describes the temperature window for reduction of surface oxide layers on ferrous powder using the current thermogravimetric setup. The significant shift to lower reduction temperatures for CrA/CrM compared to ASC100.29, detailed in Figs. 2 and 4, here translates to a shift to higher $1/T_m$ values. The peak temperatures are plotted according to Eq. 1 which gives the activation energies of reduction as the slopes of the respective curves. A change in slope, with reference to plain ASC100.29 and Fe_2O_3 which show similar apparent activation energies, can be observed for CrA and CrM as well as for the re-oxidized CrA, CrM and ASC100.29 powder. This signifies that the reduction behaviour of the oxide layer is influenced both by alloying with chromium, as has been shown to influence iron oxide stability [24], and by the initial condition of the as-received powder. It is also possible that trace elements in the powder, such as manganese which is often present in this type of plain iron powder [2], may influence the oxide layer stability and act to delay the reduction of ASC100.29 relative that of Fe_2O_3. The apparent activation energy values from the Kissinger analyses are presented in Table 2.

Table 2
Calculated E_a from Kissinger plots.

Powder grade and conditions	Activation energy (kJ/mol)	R^2
$Fe_2O_3 \rightarrow Fe_3O_4$	101 ± 5	0.99
ASC100.29	100 ± 4	0.99
Re-oxidized	63 ± 6	0.98
CrA	75 ± 4	0.99
Re-oxidized	60 ± 8	0.95
CrM	74 ± 6	0.98
Re-oxidized	69 ± 4	0.99

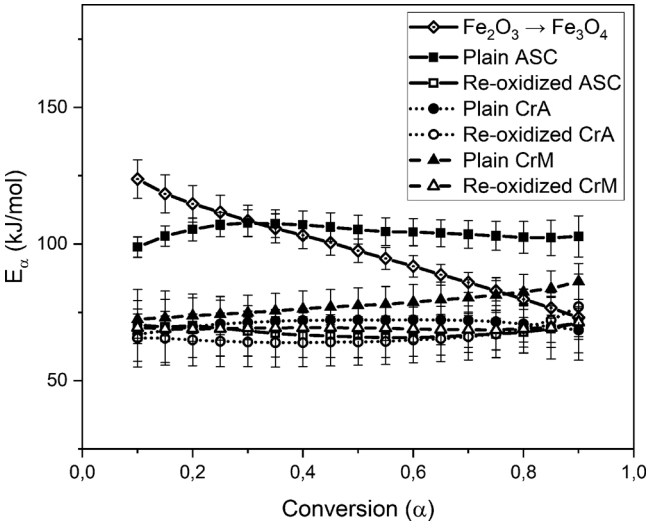

Fig. 8. Isoconversional analyses of $Fe_2O_3 \rightarrow Fe_3O_4$ and the different powder grades in their as-received and re-oxidized conditions.

The isoconversional kinetic analyses describe the reduction kinetics based on the extent of conversion and gives the possibility to reveal complex kinetic behaviours should they exist. The results of the analyses are shown in Fig. 8. The curves show a clear decrease in apparent activation energy for the plain chromium-alloyed powder grades relative to that of plain iron powder across the entire conversion range. Up to 40 kJ/mol difference in apparent activation energy is observed with CrA showing the lowest values. The Fe_2O_3 reference powder, analysed for the reaction step $Fe_2O_3 \rightarrow Fe_3O_4$, initially shows a large activation energy which continuously decreases with extent of conversion. This is in line with previous studies of reduction of Fe_2O_3 where the $Fe_2O_3 \rightarrow Fe_3O_4$ reduction step is associated with high activation energies followed by a decrease in activation energy with extent of conversion to Fe. The decrease signals a transition of the reaction from a limiting step with high activation energy to a step with lower activation energy [16,17]. Since the surface oxide layer on iron powder is expected to be mostly Fe_2O_3, the activation energies can be expected to be similar to the pure Fe_2O_3 powder. The differences observed here are believed to be twofold. Primarily, a nucleation and growth model can explain a gradual lowering of the apparent activation energy with conversion for the Fe_2O_3 reduction [16,17]. While this can likely describe the behaviour of the reduction of the micron-sized pure oxide powder, the nanometre thin oxide layers on ferrous powder grades seem to not follow this model and instead have a relatively constant apparent activation energy over the conversion range. This behaviour indicates that the reduction of the surface oxide layer is likely a single-step reaction with little to no contribution from multiple limiting steps in the reduction that could contribute to a variation of the apparent activation energy with conversion [13,16]. Secondly, there can be difficulties in separating the steps in the reduction $Fe_2O_3 \rightarrow Fe_3O_4 \rightarrow FeO \rightarrow Fe$ and choosing a proper conversion interval as overlapping and simultaneous reactions will occur, especially at the higher heating

rates. This situation can be seen in Fig. 4c-d where it becomes increasingly difficult to separate and isolate the $Fe_2O_3 \rightarrow Fe_3O_4$ reduction step.

In Fig. 8 the reduction of plain ASC100.29, CrA and CrM are also compared to their respective reduced and re-oxidized states. It can be seen that for ASC100.29, a significant lowering of the apparent activation energy is attained for the reduction of the native oxide layer formed on the re-oxidized powder. The difference is believed to be partly explained by the thinner oxide on the re-oxidized powder (3 nm vs 5−7 nm for the as-received powder), but effects originating from the structure or composition of the oxide layer cannot be disregarded and likely play a major role in affecting the reduction. Since only ASC100.29 exhibits this lowering of apparent activation energy, it is once again indicated that the oxide layer on this as-received powder is in a significantly different initial state than the chromium-alloyed grades. Meanwhile, CrA and CrM does not show this behaviour and practically no differences between the as-received and re-oxidized states could be observed. While the apparent activation energies of as-received CrA and CrM and the re-oxidized states are similar as seen in Fig. 8, it should be pointed out that the reduction temperatures still differ significantly as indicated in Figs. 6–7. The results from the iso-conversional analysis show relatively good correlation to the Kissinger method, and is in reasonable agreement with literature values for iron oxide reduction; see for example Pineau et al. [31] for a list of values. However, large variations exist as a function of the initial conditions of the samples, as well as several details regarding the experimental setup [26,31]. Nevertheless, with constant conditions in the thermogravimetric analyser as in this case, it is expected that any changes that originate from differences in the samples can be analysed and compared.

To summarize the thermogravimetric and kinetic analyses, the origin of the differences in reduction temperature and apparent activation energy between powder grades is believed to be connected to two different mechanisms; (i) a Cr cation doping effect for the oxide layer [24] possibly in conjunction with the effect of other impurity elements [26–29], which may account for the observed differences between iron and steel powder, and (ii) a large change in surface oxide characteristics of the as-received condition of the powder compared to its reduced and re-oxidized state. These results suggest that the powder production, annealing and handling leads to specific properties of the oxide layer, such as variations in oxide structure and composition, that will influence its reduction.

3.4. Surface analysis

The results from the thermal analyses indicate a potential influence of chromium on the reduction properties of the surface oxide layer. A significant decrease in reduction temperature, isothermal reduction and apparent activation energy can be observed, c.f. Figs. 2–3 and 7−8. However, it remains unclear to what extent chromium is present in the oxide layer and if it reflects the alloy composition [7], and how the presence of chromium can affect the reduction. To investigate this, the gradual reduction of the surface oxide layer on the CrA powder was tracked by sampling powder at intermediate temperatures throughout the reduction process, see Fig. 9a. At each temperature, the powder was analysed by XPS to reveal any changes in the Fe 2p and Cr 2p regions of the spectra (9b-c). It should be noted that the powder samples were exposed to air while transferring them between the thermogravimetric analyser and the XPS. Still, from the comparison of the XPS analyses, it can be seen that the oxide layer thickness on as-received powder is greater than that of native oxide and that there is a significant change in the presence of Cr oxide during the gradual reduction of the oxide layer. To detect any metallic Fe from below an oxide layer, the layer must be practically smaller than three times the attenuation length of the oxide, which for Fe 2p would be about 4.5 nm. It can be seen that at 250 °C, there is practically no metallic iron shoulder on the iron oxide peak (9b), whereas at increasing temperatures, the shoulder grows which indicates that the oxide layer thickness is reduced. At 400 °C, the oxide layer reduction is complete (9a), and the metallic iron shoulder should correspond to an oxide thickness of around 3 nm [30]. Meanwhile, the chromium oxide content is seen to increase at each step of the reduction process, indicating a growth (9c). At temperatures below 400 °C, significant diffusion of chromium from inside the powder is not likely even if a certain supply cannot be disregarded. Consequently, part of the chromium oxide comes from the oxide layer itself. It is suggested that the oxide layer is mainly Fe_2O_3 on iron powder but that small amounts of solute Cr is contained in the oxide layers of the chromium-alloyed powder grades CrA and CrM. This results in the formation and clustering of Cr oxide when heating in a reducing atmosphere already below 400 °C, in addition to the minor amount of oxide particulates that are already present on the as-received powder surfaces which are not affected by the heating to the temperatures studied in this work. This situation can be expected since any Cr solutes in a predominantly Fe_2O_3 layer will likely not be reduced alongside the oxide layer itself at low temperatures as the thermodynamic requirements for reduction of Cr_2O_3 are unfulfilled, thus leaving Cr oxide residuals on the particle surfaces.

4. Conclusions

The surface oxide layers covering water-atomized iron and steel powder have been studied using thermogravimetric and surface analysis methods. The oxide layer on the nominally pure iron powder ASC100.29 was shown to be reduced at just below 400 °C under dynamic conditions at 10 °C/min in high-purity hydrogen. A large temperature shift of the reduction rate maxima between ASC100.29 and the chromium pre-alloyed grades CrA and CrM was observed, with the maxima located at 396, 317 and 335 °C for ASC100.29, CrA and CrM, respectively. Isothermal measurements also showed a large difference between the iron and steel powder grades, with complete reduction at 300 °C achieved within 90 and 15−25 min for the iron and steel powder, respectively. These results indicate a potential effect of chromium on the oxide layer reduction behaviour. Repeated thermogravimetric experiments showed that the native oxides formed on freshly reduced powder surfaces are reduced at significantly lower temperatures than the oxide layers that constitute the initial condition of the as-received commercial powder grades. While the initial oxide thickness of as-received powder is greater, additional differences in oxide composition and structure originating from powder production, processing and handling, and their influence on reduction behaviour cannot be disregarded. Kinetic analyses further highlighted the differences between the iron powder and the two chromium-alloyed grades. An overall lowering of the apparent activation energy for oxide layer reduction by up to 40 kJ/mol could be observed for CrA and CrM compared to the reduction of plain iron powder and the Fe_2O_3 reference powder. Reduction of re-oxidized powder also lead to a similar lowering of the apparent activation energy for ASC100.29 while there were no observed differences between as-received and re-oxidized CrA and CrM.

Surface analysis by means of XPS showed an increase in chromium oxide during the gradual reduction of the oxide layer on CrA, which implies that cationic Cr was contained in the oxide layer and then precipitated in the form of Cr oxide during reduction of the low-stability iron oxide. Only small amounts of chromium can be expected to diffuse out from the matrix at these low temperatures and contribute only partly to the observed Cr oxide. The chromium oxide that remains on the powder surface after reduction of the oxide layer likely forms small nuclei that can grow further during the heating stage of sintering, with possible detrimental effects on oxide inclusions in developing sinter necks if not reduced at higher temperatures.

Clearly, there are significant differences in the kinetics of oxide reduction for various water-atomized iron and steel grades that reflect

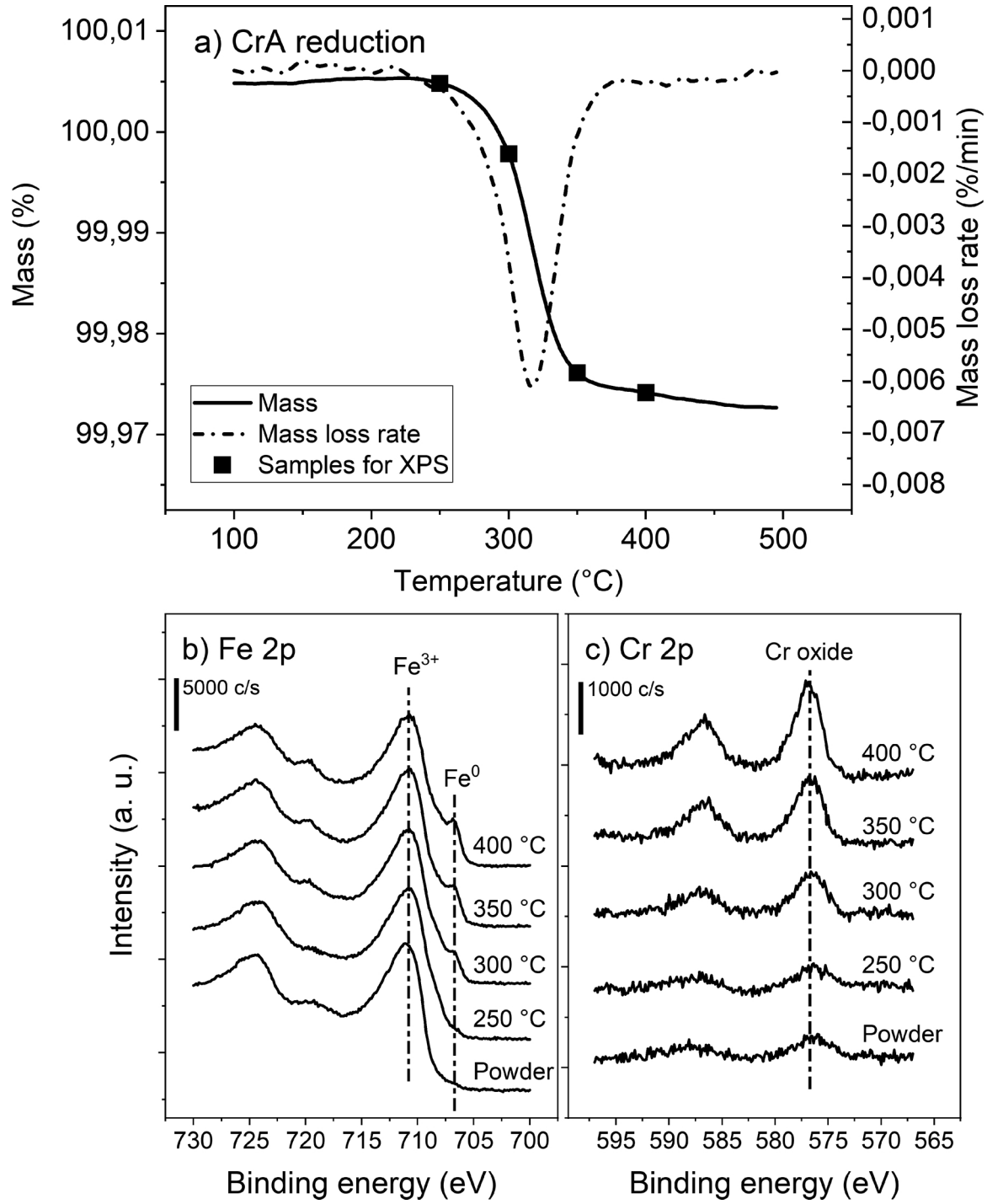

Fig. 9. Thermogravimetric reduction of CrA powder and sampling points at intermediate temperatures for XPS analysis. a) TG/DTG curves, b) Fe 2p and c) Cr 2p regions of the XPS spectra at the sampling temperatures.

the initial conditions of the powder as well as the powder and oxide chemistry.

CRediT authorship contribution statement

Johan Wendel: Conceptualization, Methodology, Investigation, Formal analysis, Writing - original draft. **Swathi K. Manchili:** Conceptualization, Investigation. **Eduard Hryha:** Conceptualization, Writing - review & editing, Supervision. **Lars Nyborg:** Conceptualization, Writing - review & editing, Supervision, Project administration, Funding acquisition.

Declaration of Competing Interest

The authors declare that they have no known competing financial interests or personal relationships that could have appeared to influence the work reported in this paper.

Acknowledgements

This work has been carried out within the project “Nanotechnology Enhanced Sintered Steel Processing” through support from the Swedish Foundation for Strategic Research under grant GMT14-0045 within the

program “Generic Methods and Tools for Future Production” and with support from Production Area of Advance at Chalmers University of Technology. Höganäs AB, Sweden, is greatly acknowledged for supplying the powder and scientific cooperation.

Appendix A. Supplementary data

Supplementary material related to this article can be found, in the online version, at doi:https://doi.org/10.1016/j.tca.2020.178731.

References

[1] E. Hryha, L. Nyborg, Oxide transformation in Cr-Mn-prealloyed sintered steels: thermodynamic and kinetic aspects, Metall. Mater. Trans. A Phys. Metall. Mater. Sci. 45 (2014) 1736–1747, https://doi.org/10.1007/s11661-013-1969-3.
[2] J. Wendel, R. Shvab, Y. Cao, E. Hryha, L. Nyborg, Surface analysis of fine water-atomized iron powder and sintered material, Surf. Interface Anal. 50 (2018) 1065–1071, https://doi.org/10.1002/sia.6455.
[3] D. Chasoglou, E. Hryha, M. Norell, L. Nyborg, Characterization of surface oxides on water-atomized steel powder by XPS/AES depth profiling and nano-scale lateral surface analysis, Appl. Surf. Sci. 268 (2013) 496–506, https://doi.org/10.1016/j.apsusc.2012.12.155.
[4] D. Chasoglou, E. Hryha, L. Nyborg, Effect of process parameters on surface oxides on chromium-alloyed steel powder during sintering, Mater. Chem. Phys. 138 (2013) 405–415, https://doi.org/10.1016/j.matchemphys.2012.11.074.
[5] D. Chasoglou, E. Hryha, L. Nyborg, Effect of Sintering Atmosphere on the Transformation of Surface Oxides During the Sintering of Chromium Alloyed Steel 9 (2009), pp. 141–155.
[6] C. Gierl-Mayer, R. de Oro Calderon, H. Danninger, The role of oxygen transfer in sintering of low alloy steel powder compacts: a review of the “Internal getter” effect, JOM 68 (2016), https://doi.org/10.1007/s11837-016-1819-z.
[7] I. Olefjord, Esca-studies of the composition profile of low temperature oxide formed on chromium steels-I, Oxydation in dry oxygen, Corros. Sci. 15 (1975) 687–696, https://doi.org/10.1016/0010-938X(75)90033-5.
[8] E. Hryha, C. Gierl, L. Nyborg, H. Danninger, E. Dudrova, Surface composition of the steel powders pre-alloyed with manganese, Appl. Surf. Sci. 256 (2010) 3946–3961, https://doi.org/10.1016/j.apsusc.2010.01.055.
[9] R. de Oro Calderon, C. Gierl-Mayer, H. Danninger, Application of thermal analysis techniques to study the oxidation/reduction phenomena during sintering of steels containing oxygen-sensitive alloying elements, J. Therm. Anal. Calorim. 127 (2017) 91–105, https://doi.org/10.1007/s10973-016-5508-5.
[10] E. Hryha, J. Wendel, Effect of heating rate and process atmosphere on the thermodynamics and kinetics of the sintering of pre-alloyed water-atomized powder metallurgy steels, J. Am. Ceram. Soc. 102 (2018) 748–756, https://doi.org/10.1111/jace.16079.
[11] H. Danninger, C. Gierl, S. Kremel, G. Leitner, Y. Yu, Degassing and deoxidation processes during sintering of unalloyed and alloyed pm steels, Powder Metall. Prog. 2 (2002) 125–140.
[12] H.E. Kissinger, Reaction kinetics in differential thermal analysis, Anal. Chem. 29 (1957) 1702–1706, https://doi.org/10.1021/ac60131a045.
[13] S. Vyazovkin, A.K. Burnham, J.M. Criado, L.A. Pérez-Maqueda, C. Popescu, N. Sbirrazzuoli, ICTAC kinetics committee recommendations for performing kinetic computations on thermal analysis data, Thermochim. Acta 520 (2011) 1–19, https://doi.org/10.1016/j.tca.2011.03.034.
[14] D. Jelić, J. Penavin-Škundrić, D. Majstorović, S. Mentus, The thermogravimetric study of silver(I) oxide reduction by hydrogen, Thermochim. Acta 526 (2011) 252–256, https://doi.org/10.1016/j.tca.2011.10.001.
[15] B. Jankovic, B. Adnadevic, S. Mentus, The kinetic study of temperature-programmed reduction of nickel oxide in hydrogen atmosphere, Chem. Eng. Sci. 63 (2008) 567–575, https://doi.org/10.1016/j.ces.2007.09.043.
[16] P. Pourghahramani, E. Forssberg, Reduction kinetics of mechanically activated hematite concentrate with hydrogen gas using nonisothermal methods, Thermochim. Acta 454 (2007) 69–77, https://doi.org/10.1016/j.tca.2006.12.023.
[17] G.Y. Lee, J. ll Song, J.S. Lee, Reaction kinetics and phase transformation during hydrogen reduction of spherical Fe2O3 nanopowder agglomerates, Powder Technol. 302 (2016) 215–221, https://doi.org/10.1016/j.powtec.2016.07.038.
[18] J. Wendel, S.K. Manchili, E. Hryha, L. Nyborg, J. Wendel, Oxide reduction and oxygen removal in water - atomized iron powder : a kinetic study, J. Therm. Anal. Calorim. (2020), https://doi.org/10.1007/s10973-020-09724-6.
[19] E. Hryha, L. Cajkova, E. Dudrova, L. Nyborg, Study of reduction/oxidation processes in Cr-Mo prealloyed steels during sintering by continuous atmosphere monitoring, Powder Metall. Prog. 7 (2007) 181–197.
[20] L.N. Samuelsson, R. Moriana, M.U. Babler, M. Ek, K. Engvall, Model-free rate expression for thermal decomposition processes: The case of microcrystalline cellulose pyrolysis, Fuel 143 (2015) 438–447, https://doi.org/10.1016/j.fuel.2014.11.079.
[21] E. Hryha, L. Nyborg, Thermogravimetry study of the effectiveness of different reducing agents during sintering of Cr-prealloyed PM steels, J. Therm. Anal. Calorim. 118 (2014) 825–834, https://doi.org/10.1007/s10973-014-3915-z.
[22] H. Asteman, R. Norling, J.E. Svensson, A. Nylund, L. Nyborg, Quantitative AES depth profiling of iron and chromium oxides in solid solution, (Cr1-xFex)2O3, Surf. Interface Anal. 34 (2002) 234–238, https://doi.org/10.1002/sia.1290.
[23] H. Danninger, C. Gierl, New alloying systems for ferrous powder metallurgy precision parts, Sci. Sinter. 40 (2008) 33–46, https://doi.org/10.2298/SOS0801033D.
[24] T.S.T. Saharuddin, A. Samsuri, F. Salleh, R. Othaman, M. Bin Kassim, M.W. Mohamed Hisham, M.A. Yarmo, Studies on reduction of chromium doped iron oxide catalyst using hydrogen and various concentration of carbon monoxide, Int. J. Hydrogen Energy 42 (2017) 9077–9086, https://doi.org/10.1016/j.ijhydene.2016.08.151.
[25] M.J. Tiernan, P.A. Barnes, G.M.B. Parkes, Reduction of iron oxide catalysts: the investigation of kinetic parameters using rate perturbation and linear heating thermoanalytical techniques, J. Phys. Chem. B 105 (2001) 220–228, https://doi.org/10.1021/jp003189+.
[26] D. Spreitzer, J. Schenk, Reduction of Iron oxides with hydrogen—a review, Steel Res. Int. 90 (2019), https://doi.org/10.1002/srin.201900108.
[27] S. Geva, M. Farren, D.H.S. John, P.C. Hayes, The effects of impurity elements on the reduction of wustite and magnetite to iron in CO/CO2 and H2/H2O gas mixtures, Metall. Trans. B. 21 (1990) 743–751, https://doi.org/10.1007/BF02654253.
[28] M.V.C. Sastri, R.P. Viswanath, B. Viswanathan, Studies on the reduction of iron oxide with hydrogen, Int. J. Hydrogen Energy 7 (1982) 951–955, https://doi.org/10.1016/0360-3199(82)90163-X.
[29] R.P. Viswanath, B. Viswanathan, M.V.C. Sastri, Hydrogen spillover effects in the reduction of iron oxide, React. Kinet. Catal. Lett. 2 (1975) 51–56, https://doi.org/10.1007/BF02060952.
[30] S. Suzuki, Y. Ishikawa, M. Isshiki, Y. Waseda, Native oxide layers formed on the surface of ultra high-purity iron and copper investigated by angle resolved XPS, Mater. Trans. JIM. 38 (1997) 1004–1009, https://doi.org/10.2320/matertrans1989.38.1004.
[31] A. Pineau, N. Kanari, I. Gaballah, Kinetics of reduction of iron oxides by H2. Part I. Low temperature reduction of hematite, Thermochim. Acta 447 (2006) 89–100, https://doi.org/10.1016/j.tca.2007.01.014.